HHS Public Access

Author manuscript

Nat Struct Mol Biol. Author manuscript; available in PMC 2020 April 21.

Published in final edited form as:

Nat Struct Mol Biol. 2019 November ; 26(11): 994–998. doi:10.1038/s41594-019-0318-7.

Structural basis of temperature sensation by the TRP channel TRPV3

Appu K. Singh[1], **Luke L. McGoldrick**[1,2], **Lusine Demirkhanyan**[3], **Merfilius Leslie**[3], **Eleonora Zakharian**[3], **Alexander I. Sobolevsky**[1]

[1]Department of Biochemistry and Molecular Biophysics, Columbia University, New York, New York, USA.

[2]Integrated Program in Cellular, Molecular, and Biomedical Studies, Columbia University, New York, New York, USA.

[3]Department of Cancer Biology & Pharmacology, University of Illinois College of Medicine, Peoria, Illinois, USA.

Abstract

We present structures of mouse TRPV3 in temperature-dependent open, closed and intermediate states that suggest two-step activation of TRPV3 by heat. During the strongly temperature-dependent first step, sensitization, the channel pore remains closed while S6 helices undergoe α-to-π transitions. During the weakly temperature-dependent second step, channel opening, tight association of the S1–S4 and pore domains is stabilized by changes in the C-terminal and linker domains.

Temperature perception is mediated by temperature-sensitive transient receptor potential (TRP) channels, thermo-TRPs, that exhibit unusually high temperature coefficient (Q_{10}) values compared to non-temperature sensitive ion channels[1–4]. Four members of the vanilloid subfamily TRP channels are thermo-TRPs: TRPV1 and TRPV2 are activated by

Correspondence should be addressed to A.I.S. (as4005@cumc.columbia.edu).

Author Contributions: A.K.S. and A.I.S. designed the project. A.K.S., L.L.M., L.D., E.Z., and A.I.S. analyzed data. A.K.S. and L.L.M. made constructs, prepared protein samples, carried out cryo-EM data collection and processing. A.K.S. and A.I.S. built molecular models. L.D. and M.L. carried out bilayer experiments. A.K.S., L.L.M., L.D., E.Z., and A.I.S. wrote the manuscript.

Supplementary Information is linked to the online version of the paper.

Competing interests: The authors declare no competing interests

Readers are welcome to comment on the online version of the paper.

Reporting Summary

Further information on research design is available in the Nature Research Reporting Summary linked to this article.

Data Availability

Cryo-EM density maps have been deposited in the Electron Microscopy Data Bank (EMDB) under accession numbers EMD-20492 for $TRPV3_{WT}$-Closed-42°C, EMD- 20493 for $TRPV3_{WT}$-Sensitized-42°C, EMD-20494 for $TRPV3_{Y564A}$-Sensitized-4°C, EMD-20495 for $TRPV3_{Y564A}$-Sensitized-37°C, EMD-20496 for $TRPV3_{Y564A}$-Open-37°C and EMD-20497 for $TRPV3_{Y564A}$-Intermediate-37 °C. Model coordinates have been deposited in the Protein Data Bank (PDB) under accession numbers 6PVL for $TRPV3_{WT}$-Closed-42°C, 6PVM for $TRPV3_{WT}$-Sensitized-42°C, 6PVN for $TRPV3_{Y564A}$-Sensitized-4°C, 6PVO for $TRPV3_{Y564A}$-Sensitized-37°C, 6PVP for $TRPV3_{Y564A}$-Open-37 °C and 6PVQ for $TRPV3_{Y564A}$-Intermediate-37°C. All other data are available from the corresponding author upon request.

noxious heat (>43°C), while TRPV3 and TRPV4 can respond to warm temperatures (< 33°C)[5–8]. TRPV3 is predominantly expressed in skin and mediates warm and pain sensation[5,8]. Temperature-dependent activation of TRPV3 is use-dependent and hysteretic; its initial activation requires higher temperatures (>50°C), while subsequent activation can occur at lower temperatures (~33°C)[9]. Recent structures of TRPV3 have provided an insight into its architecture and ligand-dependent gating[10,11]. However, how thermo-TRPs, including TRPV3, respond to changes in temperature remains largely unknown[12–14].

We purified full-length wild-type mouse TRPV3 ($TRPV3_{WT}$) and tested its function in lipid bilayers (Methods). No $TRPV3_{WT}$ activity was detected at room temperature, while a temperature increase induced robust channel openings (Fig. 1a). At 42°C, the open probability, P_o, was ~0.36 and the conductance was weakly voltage-dependent (Fig. 1b). Consistent with the previous measurements[8,15], the strong temperature dependence of the $TRPV3_{WT}$ P_o yielded a high Q_{10} = 26.9 ± 7.4 (n = 19, Fig. 1c). We incubated purified $TRPV3_{WT}$ at different temperatures and subjected it to cryo-EM. At 42°C, data processing revealed two distinct 3D reconstructions (Extended Data Figs. 1–2, Supplementary Table 1), one representing the closed state, the other a putative sensitized state (for simplicity will be referred to as the sensitized state).

The 4.4-Å resolution closed-state structure ($TRPV3_{WT}$-Closed-42°C, Fig. 1d–e) was nearly identical to the previously determined structure at 4°C ($TRPV3_{WT}$-Closed-4°C, Extended Data Fig. 3)[11]. Indeed, the pore of $TRPV3_{WT}$-Closed-42°C is hydrophobically sealed by methionines M677 at the crossing of the pore-lining S6 transmembrane segments, which are α-helical in their entirety (Fig. 1f). Importantly, at this high temperature, the transmembrane region of $TRPV3_{WT}$-Closed-42°C retains its lipid-like densities in binding sites 1 and 2, which were identified earlier in $TRPV3_{WT}$-Closed-4°C (Extended Data Fig. 3)[11]. Because of the limited resolution, we cannot unambiguously identify these densities as lipids or determine the exact type of these putative lipids. The 4.5-Å resolution sensitized state structure ($TRPV3_{WT}$-Sensitized-42°C) shows an α-to-π transition in the middle of each S6 helix. This results in an ~100° axial rotation of the C-terminal half of S6, which becomes two helical turns longer, while the TRP helix becomes two helical turns shorter. Consequently, a different set of S6 residues face the channel pore compared to the closed state (Fig. 1g), including the highly conserved N671[16]. In $TRPV3_{WT}$-Sensitized-42°C, the side chain of each M677 points away from the pore. Nevertheless, the pore remains closed as a result of the I674 hydrophobic seal. Not observing an open conformation of $TRPV3_{WT}$ at 42°C is unsurprising because of low P_o of the channel (Fig. 1c) that requires higher temperatures for efficient activation[9,17].

To determine the structure of TRPV3 in a temperature-activated open state, we looked for constructs with increased temperature sensitivity. We tested $TRPV3_{Y564A}$, which contains a single residue substitution in the binding site 2 (Extended Data Figure 4)[11]. Presumably, Y564 is directly involved in putative lipid 2 binding; its substitution to alanine lowers affinity to the putative lipid and enhances affinity to the agonist 2-APB, which compete for the same site[11]. In lipid bilayers, this mutant channel is highly sensitized when compared to $TRPV3_{WT}$; it shows weak temperature sensitivity and is open at both 22°C and 42°C (Fig. 2a). The single-channel conductance of $TRPV3_{Y564A}$ is similar to $TRPV3_{WT}$ (Fig. 2b), but

the markedly reduced steepness of the P_o temperature dependence results in a dramatically lower Q_{10} (1.21 ± 0.20; n = 21, Fig. 2c).

We first determined $TRPV3_{Y564A}$ structure at 4°C (Extended Data Figs. 1–2) at an overall resolution of 4.1 Å, which is higher than the resolution of the previous structure[11]. Due to its high resemblance to $TRPV3_{WT}$-Sensitized-42°C, we termed this structure $TRPV3_{Y564A}$-Sensitized-4°C. The similarity in structures and single-channel conductances (Figs. 1b and 2b) justifies usage of the Y564A mutant as a reasonable qualitative model of wild type for structural and functional studies. Nonetheless, increased affinity to 2-APB[11], higher open probability and reduced temperature sensitivity of $TRPV3_{Y564A}$ compared to $TRPV3_{WT}$ suggest that their quantitative comparisons should be made with caution.

At 37°C, the majority of the $TRPV3_{Y564A}$ particles were classified into low-resolution reconstructions (Extended Data Figs. 1–2, 5), likely representing an ensemble of heterogeneous conformations. However, we determined three distinct structures comprising the minority of particles. The first, 5.18-Å resolution structure shows α-to-π transitions in its S6 helices along with a pore hydrophobically sealed by I674 (Fig. 2g), similar to $TRPV3_{WT}$-Sensitized-42°C (Fig. 1g) and $TRPV3_{Y564A}$-Sensitized-4°C (Fig. 2f). Therefore, we will refer to this structure as to $TRPV3_{Y564A}$-Sensitized-37°C.

The second, 4.48-Å resolution structure (Fig. 2d–e) has an appearently open ion channel pore (Fig. 2h). Similar to 2-APB-bound $TRPV3_{Y564A}$ structure[11], the ion conduction pathway is lined by polar or negatively-charged side chains or backbone carbonyls, and has an overall negatively-charged surface, likely important for TRPV3 cation selectivity. The pore's narrowest constriction at the intracellular gate region is defined by the side chains of I674 (interatomic distance of 9.7 Å) and is similar to the intracellular gate regions of open TRPV1[18] (9.3 Å, I679) and TRPV6[11] (9.6 Å, I575). We concluded that this structure ($TRPV3_{Y564A}$-Open-37°C) represents an open state of $TRPV3_{Y564A}$ that had been activated by heat.

The third, 4.75-Å resolution structure of $TRPV3_{Y564A}$ at 37°C exhibits C2 symmetry (Fig. 2j–k), unlike our other TRPV3 structures which have C4 symmetry. This reconstruction lacks clear density for the pore domain, presumably because of strong conformational heterogeneity. In the intracellular skirt, the C-termini of two diagonal subunits, A and C, wrap around their respective three-stranded β-sheets at intersubunit interfaces (Fig. 2l–m), similar to the closed and sensitized state structures. In contrast, the C-termini of the B and D subunits point away from the membrane plane, similar to the open state structure. This C2 symmetrical structure ($TRPV3_{Y564A}$-Intermediate-37°C) likely represents an intermediate state of the channel transitioning between the sensitized and open states.

To understand heat-induced conformational changes in TRPV3, we compared the structures of TRPV3 in the closed and sensitized states and $TRPV3_{Y564A}$ in the sensitized and open states. The three structures in the sensitized state, $TRPV3_{WT}$-Sensitized-42°C, $TRPV3_{Y564A}$-Sensitized-4°C and $TRPV3_{Y564A}$-Sensitized-37°C, superpose well overall (RMSD = 1.01–1.12 Å) and have similar pore architecture and dimensions (Figs. 1g and 2f,g,i). Therefore, we propose that they represent the same state in the temperature gating

mechanism of TRPV3. Because of low resolution, we exclude the $TRPV3_{Y564A}$-Sensitized-37°C structure from further detailed comparisons. Although all structures look grossly similar, the open state structure appears ~5 Å shorter compared to the closed and sensitized state structures and its intracellular skirt rotates ~8° clockwise, when viewed intracellularly (Fig. 3a–b). The most dramatic local conformational changes between the states occur in the transmembrane, linker and C-terminal domains.

Conformational changes in the transmembrane domain are correlated with the presence of two lipid-like densities in binding sites 1 and 2. The first density is wedged in between the extracellular part of S4 and S6 (site 1), while the second one nests in a pocket formed by the S1–S4 bundle and the C-terminal part of the TRP helix (site 2). The densities in these two sites are prominent in the closed state, become weaker in the sensitized state, and disappear completely in the open state (Fig. 3c–f). In the $TRPV3_{Y564A}$-Sensitized-4°C structure, the site 1 density disappears but another density appears in closer proximity to the S4–S5 linker (Fig. 3e). Dissociation of the site 1 density may promote S4 and S6 association (Supplementary Table 2). This transition is accompanied by S6 tilting towards S4, the α-to-π transition in S6, and consequently, the two helical turn elongation of S6, the two helical turn shortening of the TRP helix, and tilting of the TRP helix. Based on our structural results, channel opening, however, appears to not only require complete removal of the densities from sites 1 and 2, but also conformational changes in the linker and C-terminal domains.

Strikingly, the ankyrin repeat domains (ARDs) in all structures are nearly identical (RMSD = 0.43–1.07 Å, Fig. 3g–h). During the closed-to-sensitized and sensitized-to-open state transitions, the ARDs move as rigid bodies while the domains connecting them to each other and to the transmembrane domain undergo significant structural rearrangements. Among these connecting domains, the most drastic changes occur in the ARD finger 3, the AR5 helix connecting loop, the linker domain, which includes helices LH1, LH2, and pre-S1, the three-stranded β-sheet and the C-terminus. Indeed, numerous studies have revealed that mutations in these domains affect thermo-TRP temperature-dependent gating[17,19–25].

The C-terminus has been proposed to play an important role in thermo-TRP temperature-dependent gating[19–21,26]. Deletions or swapping of C-termini not only made temperature sensitivity stronger or weaker but also reversed temperature sensitivities, making heat-sensitive channels cold-sensitive and vice versa[21]. Consistently, the sensitized-to-open state transition in TRPV3 is accompanied by significant conformational changes in the C-terminus (Extended Data Fig. 6). In the closed and sensitized states, the C-terminus wraps around the 3-stranded β-sheet, while in the open state, it unwraps and projects towards the cytoplasm (Figs. 1–3). In the open state, the dissociated portion of the C-terminus is partially replaced by a 12-residue long polypeptide bound to the inter-subunit interface that likely represents a portion of the N-terminus that was unfolded and unobserved in the closed and sensitized states, although the possibility that the polypeptide density corresponds to a more distal portion of the C-terminus cannot be excluded. The C-terminus appears to function as a latch that structurally supports the closed and sensitized states and that needs to be released for the channel to open. The C-terminus interacts with residues that are conserved in the thermo-TRPVs but not in TRPV5/6 (Supplementary Fig. 1). For example, conserved

residues W739 and W742 interact with hydrophobic residues and arginine R226 in the ARDs. Mutating R226 resulted in increased channel activity[27]. Additionally, the thermo-TRPV linker domains contain an 11-residue insertion that, in our structures, interacts with the C-terminal region in both the closed and sensitized states, but not in the open state, and likely transmits conformational changes between the TMD and ARD during gating. Changes in the linker domain result in altered TRPV3 temperature-dependent gating[17,28].

Superposition of the open state structures obtained in the presence of the agonist 2-APB[11] or at high temperature (Extended Data Fig. 7a–c), shows that they are very similar (RMSD =1.01 Å) and have similar pore architectures and dimensions. However, in $TRPV3_{Y564A}$-Open-37°C, the 2-APB binding pockets are unoccupied (Extended Data Fig. 7d–f). It appears that 2-APB and heat activate TRPV3 via similar mechanisms; both lead to S4 and S6 interactions and the release of the C-terminal latch. Better understanding of these mechanisms and the role of lipids in temperature sensation by TRPV3 and thermo-TRPs in general awaits further investigation.

Methods

Construct

The full-length mouse $TRPV3_{WT}$ (residues 1–825) was cloned into a pEG BacMam vector[31], with the C-terminal thrombin cleavage site (LVPRG) followed by the streptavidin affinity tag (WSHPQFEK) as was done previously for TRPV3[11]. $TRPV3_{Y564A}$ construct was produced using standard mutagenesis procedure.

Expression and purification

TRPV3 constructs were expressed and purified as was done previously for TRPV3 with minor differences[11]. Bacmids and baculoviruses were produced as described in the literature[31]. In short, baculovirus was made in Sf9 cells for ~72 hours (Thermo Fisher Scientific, mycoplasma test negative, GIBCO #12659017) and was applied to the suspension adapted HEK 293S cells lacking *N*-acetyl-glucosaminyltransferase I ($GnTI^-$, mycoplasma test negative, ATCC #CRL-3022) that were maintained in Freestyle 293 media (Gibco-Life Technologies #12338–018) supplemented with 2% FBS in presence of 5% CO_2. The cells were cultured at 37°C for ~10 hours with a baculovirus, after which 10 mM sodium butyrate was added to the cells with a concurrent reduction in temperature to 30°C. 48–60 hours post-transduction, the cells were pelleted by centrifugation at 5,471 *g* for 15 min using a Sorvall Evolution RC Centrifuge (Thermo Scientific), washed in phosphate buffer saline (PBS) pH 8.0, and pelleted again by centrifugation at 3,202 *g* for 10 min using an Eppendorf Centrifuge 5810. After resuspension in buffer (50 ml per 800 ml of culture) containing 150 mM NaCl, 20 mM Tris-HCl (pH 8.0), 1 mM βME (β-mercaptoethanol) and protease inhibitors (0.8 μM aprotinin, 2 μg/ml leupeptin, 2 μM pepstatin A and 1 mM phenylmethylsulfonyl fluoride) the cells were subjected to sonication with a Misonix sonicator (12 × 15 s, power level 8). After sonication, the cell lysate was cleared by slow speed centrifugation and the resulting supernatant was subjected to ultracentrifugation in a Beckman Coulter ultracentrifuge using Beckman Coulter Type Ti-45 rotor at 186,000 *g* for 1 hour to pellet the membranes. The membranes were mechanically homogenized and

solubilized for ~2 hours in buffer containing 150 mM NaCl, 20 mM Tris-HCl pH 8.0, 1% digitonin and 1 mM βME. The mixture was subjected to ultracentrifugation for 1 hour at 186,000 *g* to remove any remaining insoluble material. The supernatant was added to a streptavidin-linked resin and rotated for 10–14 hours at 4°C. The resin was washed with 10 column volumes of wash buffer containing 150 mM NaCl, 20 mM Tris-HCl pH 8.0, 1 mM BME and 0.01% GDN and the protein was eluted with the same buffer supplemented with 2.5 mM D-desthiobiotin. All constructs were further purified by size-exclusion chromatography using a Superose 6 column equilibrated in 150 mM NaCl, 20 mM Tris-HCl pH 8.0, 1mM βME and 0.01% GDN. Tris(2-carboxyethyl)phosphine (TCEP, 10 mM) was added to the tetrameric peak fractions which were pooled together and concentrated to ~4.5 mg/ml.

Cryo-EM sample preparation and data collection

Au/Au grids were prepared as described in the literature[32]. Briefly, grids were prepared by first coating C-flat (Protochips, Inc., Morrisville, NC) CF-1.2/1.3–2Au mesh holey carbon grids with ~60 nm of gold using an Edwards Auto 306 evaporator. Subsequently, an Ar/O_2 plasma treatment (4 min, 50 watts, 35.0 sccm Ar, 11.5 sccm O_2) was used to remove the carbon with a Gatan Solarus (model 950) Advanced Plasma Cleaning System. The grids were again plasma treated (H_2/O_2, 20 s, 10 watts, 6.4 sccm H_2, 27.5 sccm O_2) prior to sample application in order to make their surfaces hydrophilic. A 3-μl protein solution was applied on the gold side of the grid and then the sample was blotted for 2 s with a blot force of 3, and a wait time of 20 s. Subsequently, the grid was plunge frozen in liquid ethane using Vitrobot Mark V1 that was set to 100% humidity and 42°C for $TRPV3_{WT}$-42°C, 4 °C for $TRPV3_{Y564A}$-4°C, and 37 °C for $TRPV3_{Y564A}$-37°C. To get structures of TRPV3 at the corresponding temperatures, the purified protein samples were kept at 42°C for $TRPV3_{WT}$-42°C and 37 °C for $TRPV3_{Y564A}$-37°C for a maximum of 4–5 min prior to applying on grids. Incubation of $TRPV3_{WT}$ at 48°C resulted in grids with non-vitreous ice and, as a result, precluded particle visualization using cryo-EM. However, incubation of $TRPV3_{WT}$ grids at 42°C prior to plunge freezing resulted in vitreous ice and ultimately, high-resolution 3D reconstructions (Extended Data Figs. 1–2, Supplementary Table 1).

The $TRPV3_{WT}$-42°C data were collected on a Thermo Fisher Scientific Titan Krios TEM (FEI) microscope operating at 300 kV equipped with a post-column GIF Quantum energy filter, and a Gatan K2 Summit direct electron detection (DED) camera (Gatan, Pleasanton, CA, USA). 6407 movies were collected in counting mode with a calibrated magnification of 130,000 that corresponds to a pixel size of 1.06 Å. The defocus range was set to −1.0 μm to −2.5 μm during dataset acquisition. For each movie, a total dose, ~57 $e^{-}Å^{-2}$, was attained by using a dose rate of ~8.0 $e\text{-}pixel^{-1}s^{-1}$ across 40 frames for 8 s total exposure time.

The $TRPV3_{Y564A}$-4°C data were collected on a Thermo Fisher Scientific Titan Krios TEM (FEI) microscope operating at 300 kV equipped with a post-column GIF Quantum energy filter, and a Gatan K2 Summit direct electron detection (DED) camera (Gatan, Pleasanton, CA, USA). 5882 movies were collected in counting mode with a calibrated magnification of 130,000 that corresponds to a pixel size of 1.06 Å. The defocus range was set to −1.0 μm to

−2.5 μm during dataset acquisition. For each movie, a total dose, ~57 $e^{-}Å^{-2}$, was attained by using a dose rate of ~8.0 e-pixel^{-1}s^{-1} across 40 frames for 8 s total exposure time.

The multiple TRPV3$_{Y564A}$-37°C data were collected on Titan Krios TEM operating at 300 kV equipped with a Gatan K2 Summit DED camera using Leginon[33]. Four Titan Krios collections, resulting in a total of 18,901 micrographs, were collected in counting mode with a pixel size of 1.06 Å. A defocus range of −1.5 μm to −3.0 μm was used and the total dose, ~57 $e^{-}Å^{-2}$, was attained by using a dose rate of 8.0 e-pixel^{-1}s^{-1} across 40 frames for 8 s total exposure time.

Image processing

All TRPV3 data were processed in Relion 3.0[34] and cryoSPARC[35]. All the movies were motion-corrected with MotionCor2 algorithm implemented in RELION. CTF estimation was performed in Gctf[36] on non-dose-weighted micrographs while subsequent data processing was done on dose-weighted micrographs.

The TRPV3$_{WT}$-42°C dataset was processed as follows. Initially, ~1000 particles were manually picked to generate 2D class templates that were subsequently used to automatically pick 1,541,116 particles. Automatically picked particles were extracted with a box size of 220 pixels in RELION 3.0[34]. The extracted particle images were subjected to 3D classification into ten classes, using the closed state structure of TRPV3 as a reference[11] (PDB: 6DVW). One class, composed of 342,688 particles, was refined with C1 symmetry and post-processed. The resulting ~5.7 Å structure was used a reference for the next round of 3D classification (with C1 symmetry) in which the ~342,688 particles were separated into another 10 classes. 2 of the resulting classes, composed of 33,741 and 50,647 particles, were refined with C4 symmetry and post-processed to generate the final 4.4 Å and 4.5 Å maps for the closed and sensitized states of TRPV3$_{WT}$-42°C. Similar processing workflow was adopted for the TRPV3$_{Y564A}$-4°C that resulted in a final 3D reconstruction at 4.07 Å resolution.

However, similar processing procedure applied to TRPV3$_{Y564A}$-37°C data resulted in ~7.0 Å resolution reconstruction, presumably because of most of the particles for this dataset were either unfolded on the grid or highly heterogeneous. Indeed, 3D classification showed both of these features in processed particles, limiting our efforts to structure determination. To increase the number of particles in the open state, we collected a total of four datasets on Titan Krios, that resulted in 18901 micrographs. The total of ~6,000,000 particles were extracted with the box size of 220 pixels. These extracted particles were subjected to multiple rounds of heterogeneous classification in RELION[34] (Extended Data Fig. 5), resulting in three major classes: TRPV3$_{Y564A}$-Open-37°C, TRPV3$_{Y564A}$-Sensitized-37°C, and TRPV3$_{Y564A}$-Intermediate-37°C. TRPV3$_{Y564A}$-Intermediate-37°C represented C2 symmetric structure in which the intracellular ankyrin repeat domain was resolved well, while the channel pore was resolved poorly.

The fraction of particles representing each state in our heterogeneous datasets yielding multiple conformations (Supplementary Table 1) does not necessarily match the representation of the corresponding states in our functional experiments (Figs. 1–2). The

reason for this discrepancy is the inherent difference between conditions of the protein sample in cryo-EM and in the lipid bilayer experiments. These include a different physical environment for the transmembrane portion of the protein (detergent micelle versus lipid bilayer) as well as protein interactions with the thin layer of vitreous ice (including surface tension effects) and possibly with the material of the grid (gold mesh). Nevertheless, despite the absolute numbers of particles in the cryo-EM datasets do not match representations of the corresponding states in functional experiments, the qualitative presence of these states is likely preserved.

The reported resolutions of the final maps were estimated using the Fourier shell correlation (FSC)=0.143 criterion[37] on masking-effect-corrected FSC curves calculated between two independent half-maps[38]. The local resolutions were estimated with unfiltered half maps using ResMap[30] and EM density visualization was done in UCSF Chimera[39].

Model building

To build the closed, sensitized and open state models of TRPV3 in COOT[40], we used the previously published cryo-EM structures of TRPV3 as guides[11]. The models were tested for overfitting (Extended Data Fig. 2) by shifting their coordinates by 0.5 Å (using shake) in PHENIX[41], refining each shaken model against a corresponding unfiltered half map, and generating densities from the resulting models in Chimera. FSC was calculated between the densities generated in Chimera and both unfiltered half maps and the sum maps, using EMAN2[42]. The local resolution of the transmembrane domains in all our reconstructions, except $TRPV3_{Y564A}$-Intermediate-37°C, was higher compared to the resolution of the soluble domains, as evidenced by local resolution predictions made using ResMap[30]. High resolution of the transmembrane domains allowed us to unambiguously define the conformation of the pore-lining S6 helices in the closed, sensitized and open state structures. Structures were visualized and figures were prepared in Chimera and Pymol[43].

Planar lipid bilayer measurements

Planar lipid bilayers measurements were performed as described previously[44]. Briefly, planar lipid bilayers were formed from a solution of synthetic 1-palmitoyl-2-oleoyl-sn-glycero-3-phospho-(1'-rac-glycerol) (POPG), 1-palmitoyl-2-oleoyl-glycero-3-phosphocoline (POPC) and 1-palmitoyl-2-oleoyl-glycero-3-phosphoethanolamine (POPE; Avanti Polar Lipids) at a 3:1:1 ratio in *n*-decane (Sigma-Aldrich). The solution was used to paint a bilayer in an aperture of ~150 μm diameter in a Delrin cup (Warner Instruments) between symmetric aqueous bathing solutions of 150 mM KCl, 0.02 mM $MgCl_2$, 1 μM $CaCl_2$, and 20 mM HEPES (pH 7.2). Unless specified otherwise, all experiments were performed in the presence of 2.5 μM 1-(1,2R-dioctanoylphosphatidyl)inositol-4,5-bisphosphate, trisodium salt (DiC_8-PIP_2, Cayman Chemical) added to both compartments. All reagents (Sigma-Aldrich) were ultrapure (>99%). Bilayer capacitances were in the range of 50–75 pF.

After the bilayers had formed, the micellar solution of TRPV3 protein (0.02 μg/ml) was added by painting. Unitary currents were recorded using the Axopatch 200B patch-clamp amplifier (Molecular Devices). The *trans* solution (command voltage side) was connected to the CV 201A head-stage input, while the *cis* solution was held at a virtual ground *via* a pair

of matched Ag-AgCl electrodes. Currents through the voltage-clamped bilayers (background conductance, <1 pS) were filtered at the amplifier output (low pass, −3 dB at 10 kHz, 8-pole Bessel response). Data were filtered at 100 Hz through an 8-pole Bessel filter (950 TAF; Frequency Devices) and digitized at 1 kHz with an analog-to-digital converter Digidata 1322A controlled by pClamp10.3 software (Molecular Devices). Single-channel conductance events, all-points histograms, open probability (P_o), and other parameters were identified and analyzed with Clampfit10.3 software (Molecular Devices). The experiments were performed in the temperature range from 22 to 42°C. For the temperature-dependence measurements, the bilayer recording chamber was fitted onto a conductive stage containing a pyroelectric heater/cooler that was controlled by a temperature controller (CL-100; Warner Instruments). Deionized water was circulated through the stage and pumped into the system to remove the generated heat. The temperature of the bath was constantly monitored using a thermoelectric device in the cis chamber (the ground side) and was reliably controlled within ±0.5°C. The temperature coefficients (Q10) for P_o were calculated using Eq. 1:

$$Q_{10} = \left(\frac{X_2}{X_1}\right)^{\frac{10}{T_2 - T_1}} \quad (1)$$

where X_1 and X_2 are P_o values obtained at T_1 and T_2 temperatures measured in Kelvins. Statistical analysis was performed using Origin 9.0 (Microcal Software Inc.). Statistical significance was calculated using One-Way ANOVA followed by Fisher's least significant difference test. All data are presented as mean ± SEM.

Extended Data

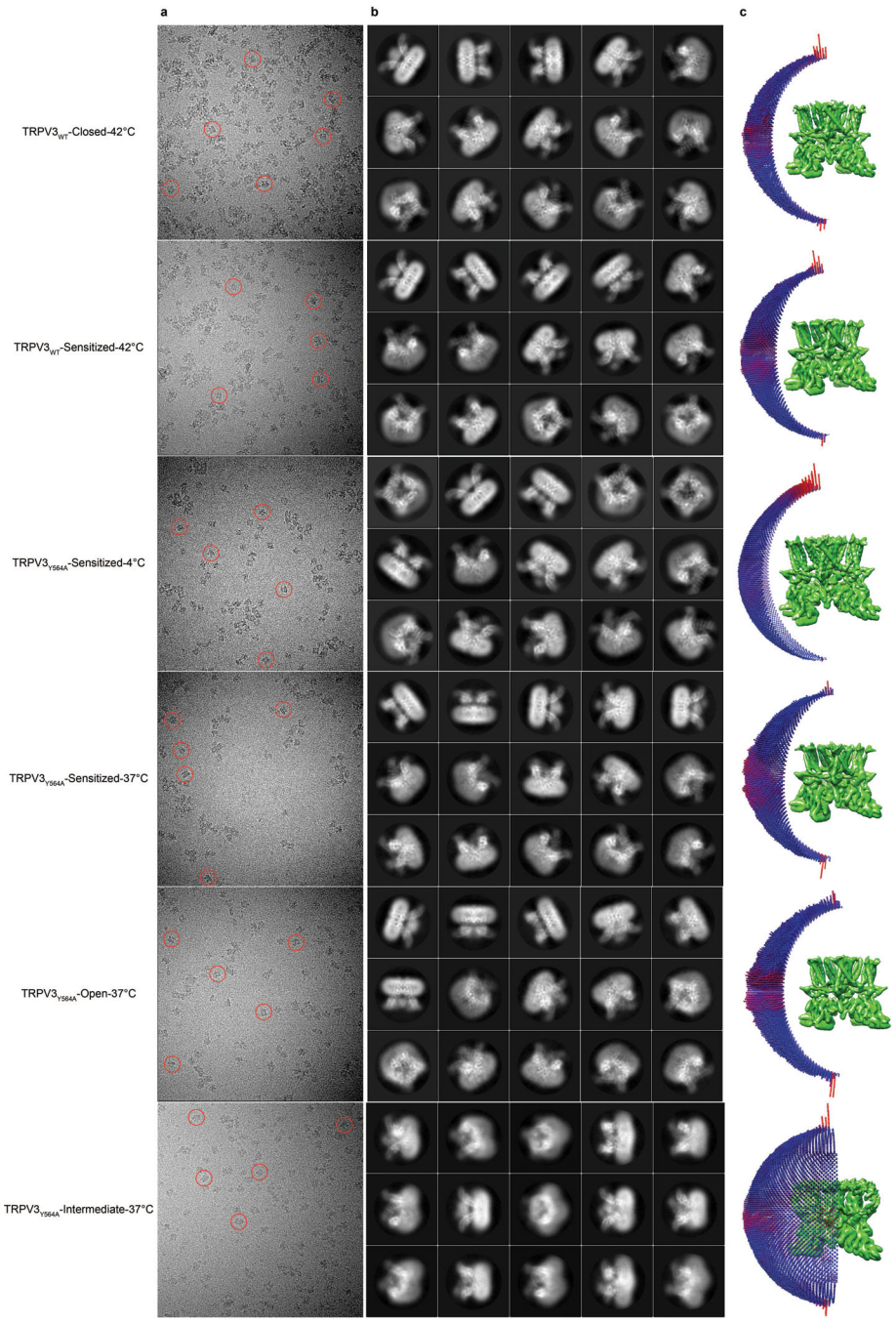

Extended Data Fig. 1. Overview of cryo-EM data collected for TRPV3$_{WT}$ and TRPV3$_{Y564A}$

Example micrographs from different TRPV3-construct collections with example particles circled in red (left column), reference-free 2D class averages in different orientations (middle column) and Euler angle distribution of particles contributing to the final reconstructions with larger red cylinders representing orientations comprising more particles (right column).

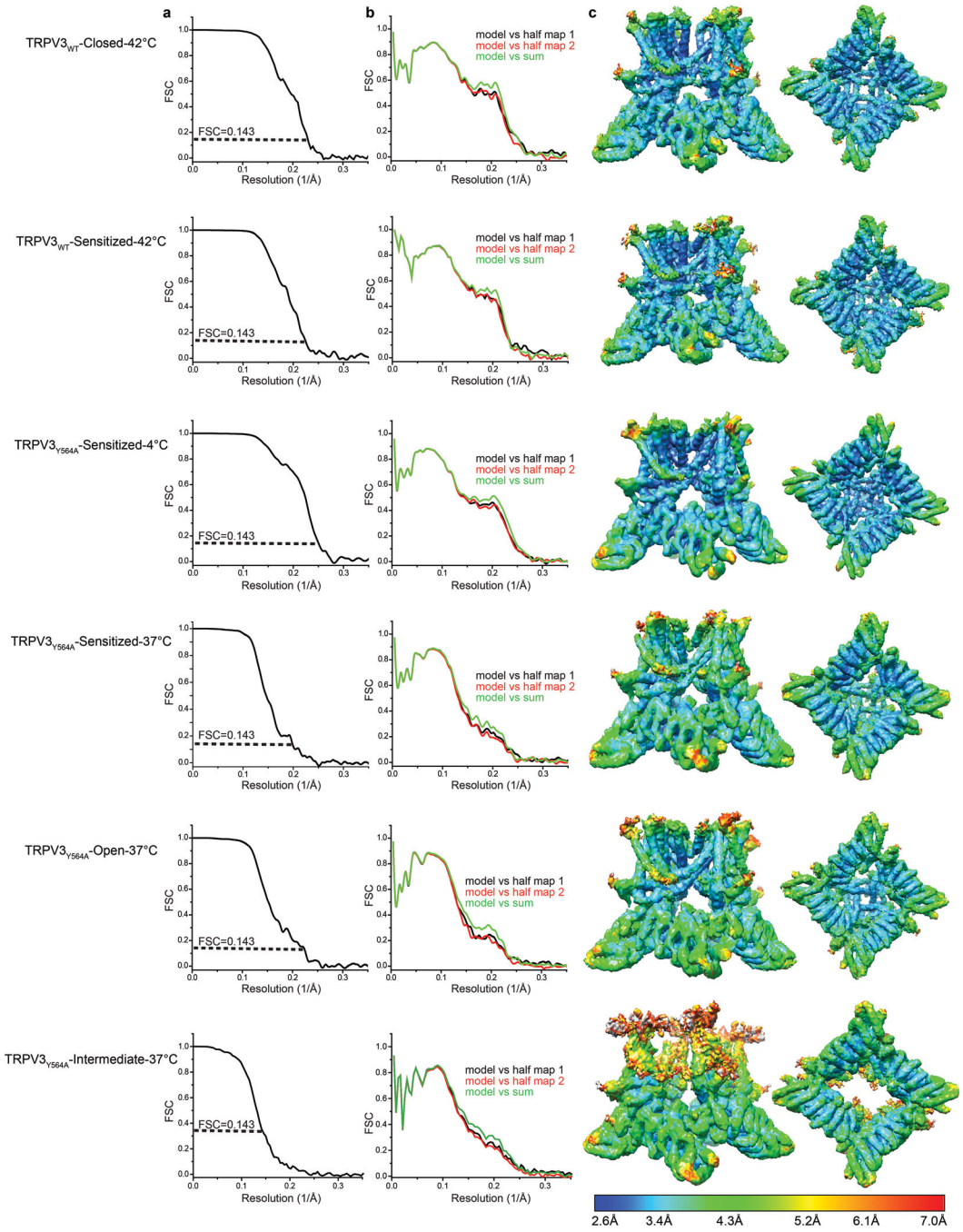

Extended Data Fig. 2. Resolution of $TRPV3_{WT}$ and $TRPV3_{Y564A}$ cryo-EM reconstructions

a, FSC curves calculated between half maps. **b**, FSC curves calculated between two unfiltered half-maps and the final map and a model whose coordinates were randomized and refined against only half map 1. **c**, Local resolution predicted by ResMap[30].

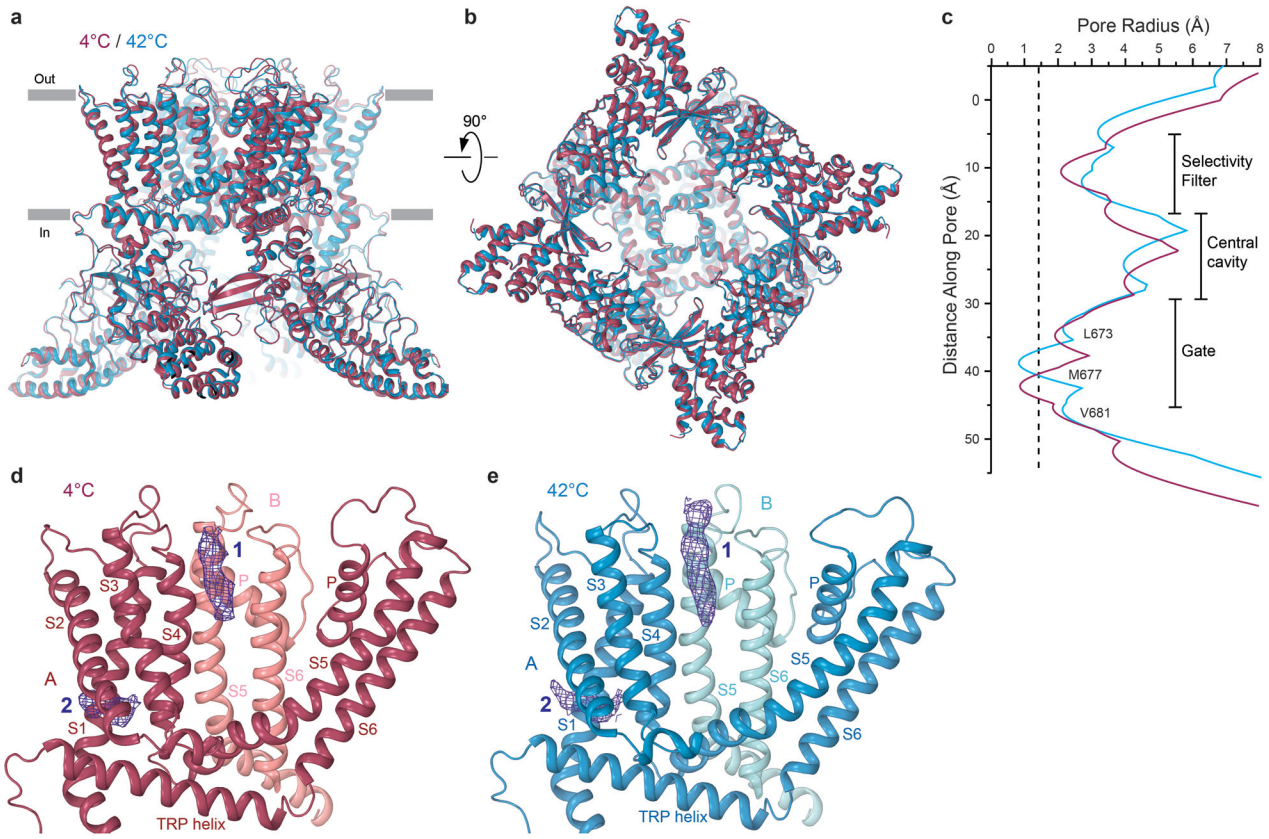

Extended Data Fig. 3. Comparison of TRPV3$_{WT}$ closed state structures at 4°C and 42°C

a–b, Overall superposition of TRPV3$_{WT}$-closed-4^{o}C (red) and TRPV3$_{WT}$-closed-42^{o}C (blue) structures viewed parallel to membrane (**a**) or intracellularly (**b**). **c**, Pore radii calculated using HOLE[29]. The vertical dashed line denotes the radius of a water molecule, 1.4 Å. **d–e**, Expanded view of the transmembrane domain of one TRPV3$_{WT}$-Closed-4^{o}C (**d**) or TRPV3$_{WT}$-Closed-42^{o}C (**e**) subunit with lipid-like densities shown as purple mesh.

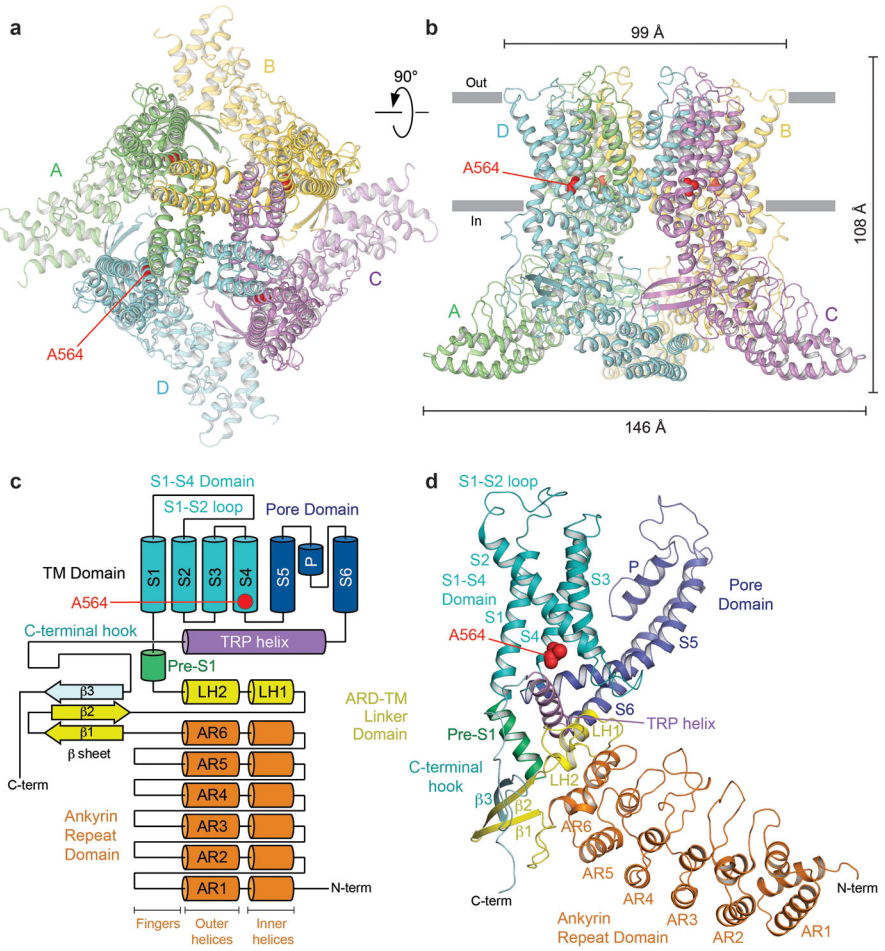

Extended Data Fig. 4. Architecture and domain organization of TRPV3

a–b, Top (**a**) and side (**b**) views of the TRPV3 tetramer, with each subunit shown in a different color. **c**, Domain organization diagram of the TRPV3 subunit. **d**, Structure of TRPV3 subunit, with domains colored as in **c**. Alanine substituting tyrosine Y564 in $TRPV3_{Y564A}$ is shown in red space-filling representation (**a**, **b** and **d**) or indicated by the red circle (**c**).

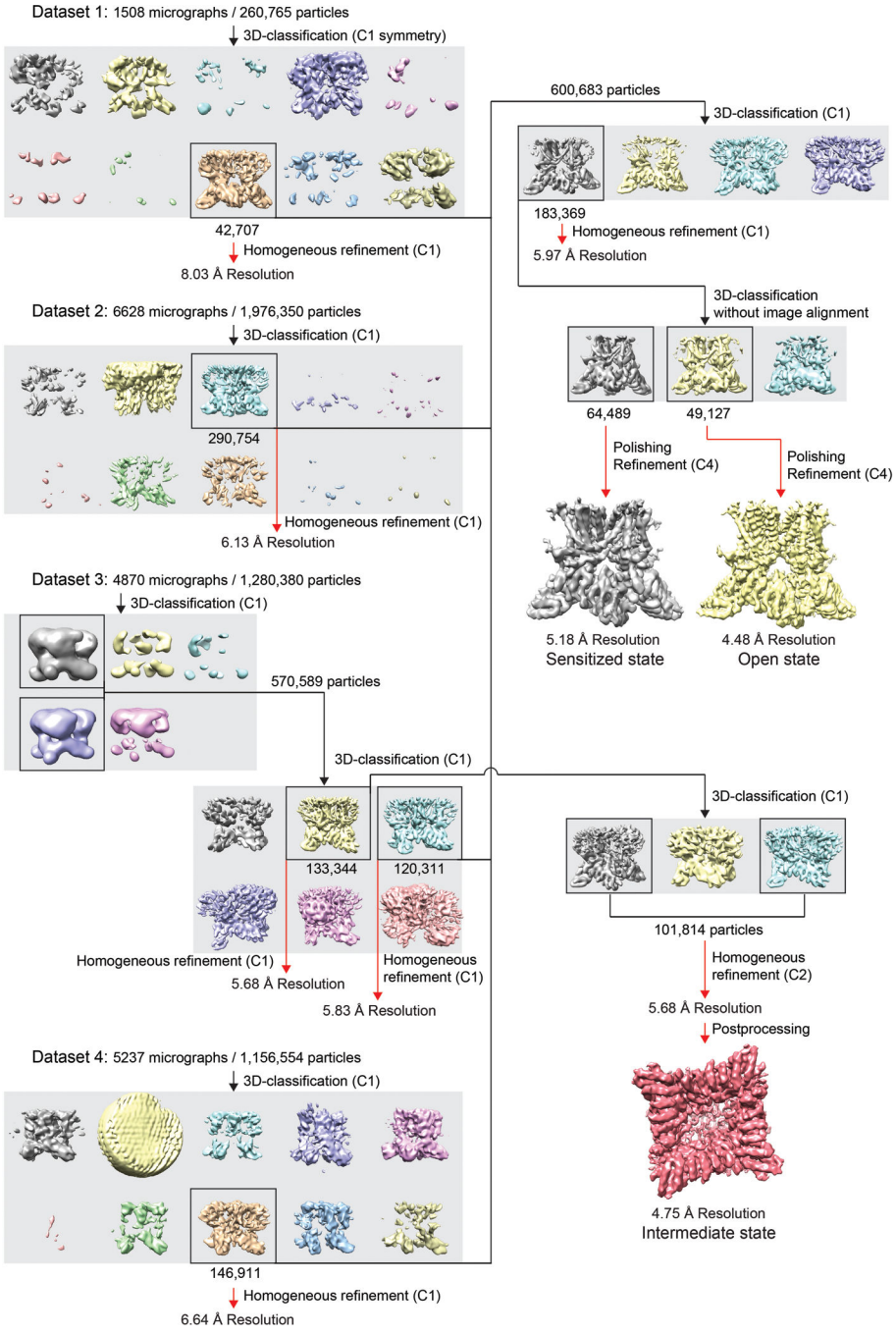

Extended Data Fig. 5. 3D reconstruction workflow

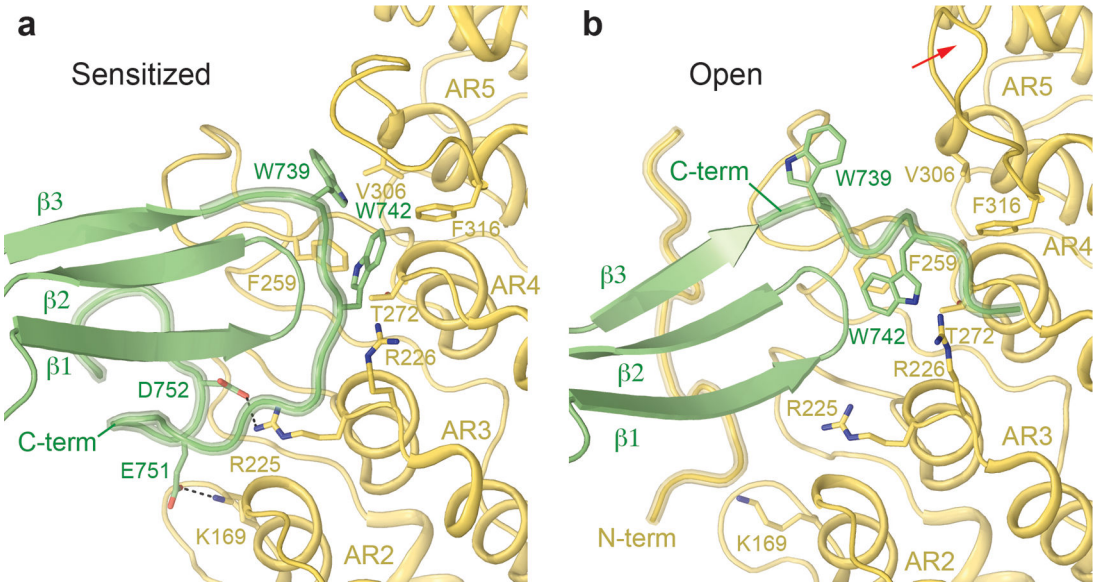

Extended Data Fig. 6. C-terminus unlatching during channel opening

a–b, Expanded view of the cytosolic inter-subunit interface in $TRPV3_{Y564A}$-Sensitized-4°C (**a**) and $TRPV3_{Y564A}$-Open-37°C (**b**). The C-termini and the putative N-terminus fragment from the $TRPV3_{Y564A}$-Open-37°C adjacent subunit are thickened for clarity. Conserved residues at the C-terminus-ARD interfaces are shown as sticks. Movement of the AR5 loop in the open state relative to the sensitized or closed state is indicated by a red arrow.

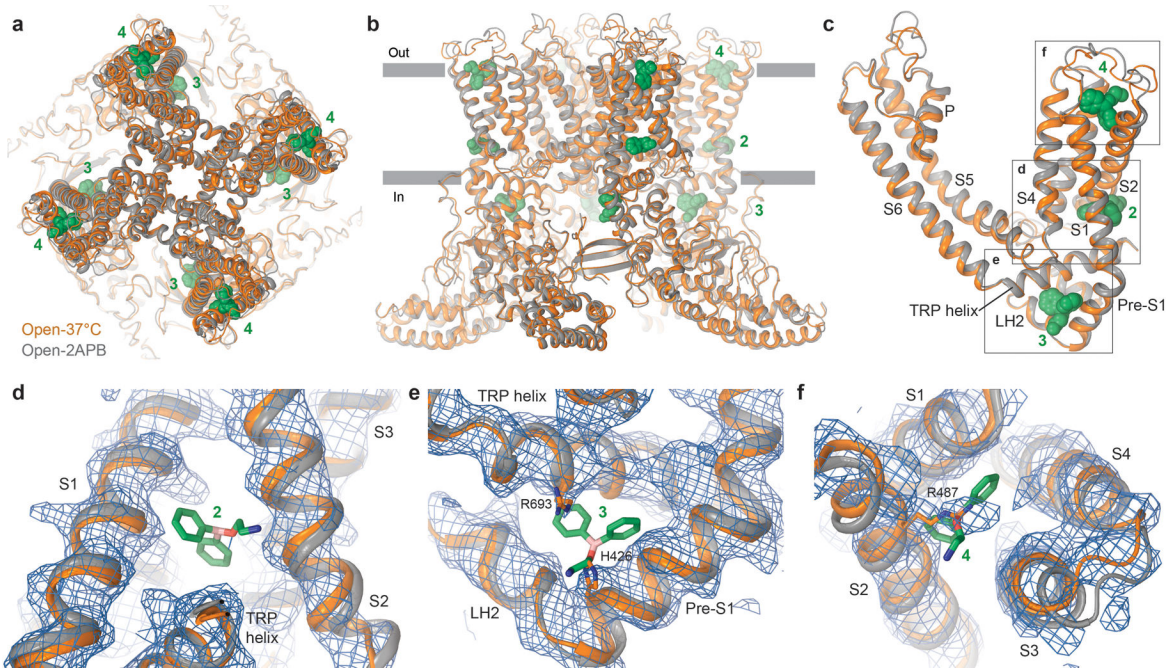

Extended Data Fig. 7. Comparison of heat- and ligand-activated open states

a–c, Overall superposition of $TRPV3_{Y564A}$-Open-37°C (orange) and $TRPV3_{Y564A}$-Open-2-APB (grey) viewed extracellularly (**a**) and parallel to membrane (**b**) and an expanded view of the transmembrane domain of one subunit (**c**). 2-APB molecules bound to $TRPV3_{Y564A}$-Open-2-APB structure are shown as space-filling models. **d-f**, Expanded views of binding sites 2 (**d**), 3 (**e**) and 4 (**f**). The 2-APB molecules bound to $TRPV3_{Y564A}$-Open-2-APB are shown as sticks and the $TRPV3_{Y564A}$-Open-37°C density is shown as blue mesh. $TRPV3_{Y564A}$-Open-37°C residues that would clash with the 2-APB molecules are shown in stick representation.

Supplementary Material

Refer to Web version on PubMed Central for supplementary material.

Acknowledgments:

We thank R. Grassucci for assistance with microscope operation, U. Baxa and T. Edwards for help with data collection, and H. Kao for computational support. We thank J. Yoder for comments on the manuscript and M. Yelshanskaya for helpful discussions. L.L.M. is supported by the NIH (F31 CA232391–01). A.I.S. is supported by the NIH (R01 CA206573, R01 NS083660, R01 NS107253), NSF (1818213) and the Irma T. Hirschl Career Scientist Award. Data were collected at the Frederick National Laboratory for Cancer Research National Cryo-EM Facility (NIH) and at the Simons Electron Microscopy Center and National Resource for Automated Molecular Microscopy (New York Structural Biology Center) supported by grants from the Simons Foundation (349247), NYSTAR and the NIH (GM103310).

References

1. Caterina MJ et al. The capsaicin receptor: a heat-activated ion channel in the pain pathway. Nature 389, 816–24 (1997). [PubMed: 9349813]
2. Patapoutian A, Peier AM, Story GM & Viswanath V Thermotrp channels and beyond: Mechanisms of temperature sensation (vol 4, pg 529, 2003). Nature Reviews Neuroscience 4, 691–691 (2003).

3. Jordt SE, McKemy DD & Julius D Lessons from peppers and peppermint: the molecular logic of thermosensation. Current Opinion in Neurobiology 13, 487–492 (2003). [PubMed: 12965298]
4. Clapham DE TRP channels as cellular sensors. Nature 426, 517–524 (2003). [PubMed: 14654832]
5. Peier AM et al. A heat-sensitive TRP channel expressed in keratinocytes. Science 296, 2046–9 (2002). [PubMed: 12016205]
6. Guler AD et al. Heat-evoked activation of the ion channel, TRPV4. J Neurosci 22, 6408–14 (2002). [PubMed: 12151520]
7. Caterina MJ, Rosen TA, Tominaga M, Brake AJ & Julius D A capsaicin-receptor homologue with a high threshold for noxious heat. Nature 398, 436–41 (1999). [PubMed: 10201375]
8. Smith GD et al. TRPV3 is a temperature-sensitive vanilloid receptor-like protein. Nature 418, 186–190 (2002). [PubMed: 12077606]
9. Liu BY, Yao J, Zhu MX & Qin F Hysteresis of gating underlines sensitization of TRPV3 channels. Journal of General Physiology 138, 509–520 (2011). [PubMed: 22006988]
10. Zubcevic L et al. Conformational ensemble of the human TRPV3 ion channel. Nat Commun 9, 4773 (2018). [PubMed: 30429472]
11. Singh AK, McGoldrick LL & Sobolevsky AI Structure and gating mechanism of the transient receptor potential channel TRPV3. Nat Struct Mol Biol 25, 805–813 (2018). [PubMed: 30127359]
12. Diaz-Franulic I, Poblete H, Mino-Galaz G, Gonzalez C & Latorre R Allosterism and Structure in Thermally Activated Transient Receptor Potential Channels. Annual Review of Biophysics, Vol 45 45, 371–398 (2016).
13. Feng Q Temperature Sensing by Thermal TRP Channels: Thermodynamic Basis and Molecular Insights. Thermal Sensors 74, 19–50 (2014).
14. Voets T Quantifying and Modeling the Temperature-Dependent Gating of TRP Channels. Reviews of Physiology, Biochemistry and Pharmacology, Vol 162 162, 91–119 (2012).
15. Xu HX et al. TRPV3 is a calcium-permeable temperature-sensitive cation channel. Nature 418, 181–186 (2002). [PubMed: 12077604]
16. Kasimova MA, Lindahl E & Delemotte L Determining the molecular basis of voltage sensitivity in membrane proteins. Journal of General Physiology 150, 1444–1458 (2018). [PubMed: 30150239]
17. Liu B & Qin F Single-residue molecular switch for high-temperature dependence of vanilloid receptor TRPV3. Proc Natl Acad Sci U S A 114, 1589–1594 (2017). [PubMed: 28154143]
18. Cao E, Liao M, Cheng Y & Julius D TRPV1 structures in distinct conformations reveal activation mechanisms. Nature 504, 113–8 (2013). [PubMed: 24305161]
19. Vlachova V et al. Functional role of C-terminal cytoplasmic tail of rat vanilloid receptor 1. J Neurosci 23, 1340–50 (2003). [PubMed: 12598622]
20. Brauchi S, Orio P & Latorre R Clues to understanding cold sensation: thermodynamics and electrophysiological analysis of the cold receptor TRPM8. Proc Natl Acad Sci U S A 101, 15494–9 (2004). [PubMed: 15492228]
21. Brauchi S, Orta G, Salazar M, Rosenmann E & Latorre R A hot-sensing cold receptor: C-terminal domain determines thermosensation in transient receptor potential channels. J Neurosci 26, 4835–40 (2006). [PubMed: 16672657]
22. Grandl J et al. Pore region of TRPV3 ion channel is specifically required for heat activation. Nature Neuroscience 11, 1007–1013 (2008). [PubMed: 19160498]
23. Grandl J et al. Temperature-induced opening of TRPV1 ion channel is stabilized by the pore domain. Nature Neuroscience 13, 708–714 (2010). [PubMed: 20414199]
24. Yao J, Liu BY & Qin F Modular thermal sensors in temperature-gated transient receptor potential (TRP) channels. Proceedings of the National Academy of Sciences of the United States of America 108, 11109–11114 (2011). [PubMed: 21690353]
25. Macikova L, Vyklicka L, Barvik I, Sobolevsky AI & Vlachova V Cytoplasmic Inter-Subunit Interface Controls Use-Dependence of Thermal Activation of TRPV3 Channel. Int J Mol Sci 20(2019).
26. Brauchi S et al. Dissection of the components for PIP2 activation and thermosensation in TRP channels. Proc Natl Acad Sci U S A 104, 10246–51 (2007). [PubMed: 17548815]

27. Shi DJ, Ye S, Cao X, Zhang RG & Wang KW Crystal structure of the N-terminal ankyrin repeat domain of TRPV3 reveals unique conformation of finger 3 loop critical for channel function. Protein & Cell 4, 942–950 (2013). [PubMed: 24248473]
28. Yao J, Liu B & Qin F Modular thermal sensors in temperature-gated transient receptor potential (TRP) channels. Proc Natl Acad Sci U S A 108, 11109–14 (2011). [PubMed: 21690353]
29. Smart OS, Neduvelil JG, Wang X, Wallace BA & Sansom MSP HOLE: A program for the analysis of the pore dimensions of ion channel structural models. Journal of Molecular Graphics & Modelling 14, 354-& (1996).
30. Kucukelbir A, Sigworth FJ & Tagare HD Quantifying the local resolution of cryo-EM density maps. Nat Methods 11, 63–5 (2014). [PubMed: 24213166]
31. Goehring A et al. Screening and large-scale expression of membrane proteins in mammalian cells for structural studies. Nat Protoc 9, 2574–85 (2014). [PubMed: 25299155]
32. Russo CJ & Passmore LA Electron microscopy: Ultrastable gold substrates for electron cryomicroscopy. Science 346, 1377–80 (2014). [PubMed: 25504723]
33. Suloway C et al. Automated molecular microscopy: the new Leginon system. J Struct Biol 151, 41–60 (2005). [PubMed: 15890530]
34. Zivanov J et al. New tools for automated high-resolution cryo-EM structure determination in RELION-3. Elife 7(2018).
35. Punjani A, Rubinstein JL, Fleet DJ & Brubaker MA cryoSPARC: algorithms for rapid unsupervised cryo-EM structure determination. Nat Methods 14, 290–296 (2017). [PubMed: 28165473]
36. Zhang K Gctf: Real-time CTF determination and correction. J Struct Biol 193, 1–12 (2016). [PubMed: 26592709]
37. Scheres SH & Chen S Prevention of overfitting in cryo-EM structure determination. Nat Methods 9, 853–4 (2012). [PubMed: 22842542]
38. Chen S et al. High-resolution noise substitution to measure overfitting and validate resolution in 3D structure determination by single particle electron cryomicroscopy. Ultramicroscopy 135, 24–35 (2013). [PubMed: 23872039]
39. Pettersen EF et al. UCSF Chimera--a visualization system for exploratory research and analysis. J Comput Chem 25, 1605–12 (2004). [PubMed: 15264254]
40. Emsley P, Lohkamp B, Scott WG & Cowtan K Features and development of Coot. Acta Crystallogr D Biol Crystallogr 66, 486–501 (2010). [PubMed: 20383002]
41. Afonine PV et al. Towards automated crystallographic structure refinement with phenix.refine. Acta Crystallographica Section D-Structural Biology 68, 352–367 (2012).
42. Tang G et al. EMAN2: an extensible image processing suite for electron microscopy. J Struct Biol 157, 38–46 (2007). [PubMed: 16859925]
43. Afonine PV et al. Towards automated crystallographic structure refinement with phenix.refine. Acta Crystallogr D Biol Crystallogr 68, 352–67 (2012). [PubMed: 22505256]
44. Zakharian E Recording of ion channel activity in planar lipid bilayer experiments. Methods Mol Biol 998, 109–18 (2013). [PubMed: 23529424]

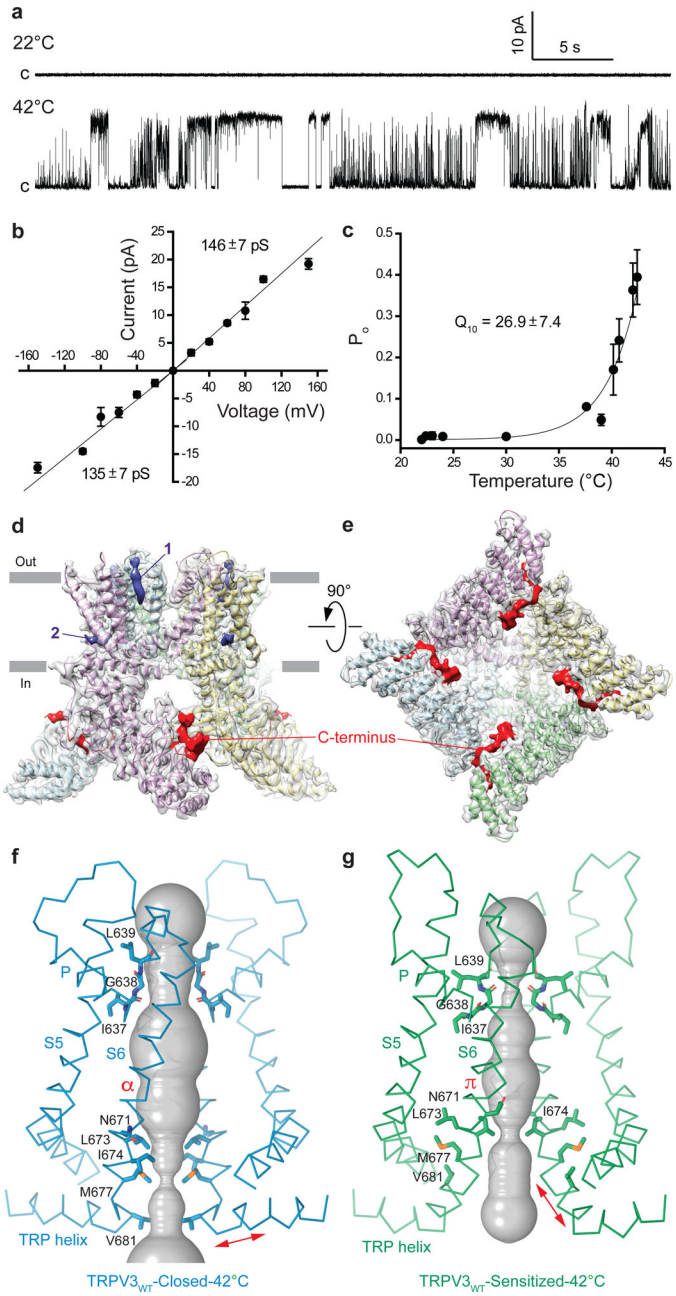

Figure 1. Functional characterization and structures of TRPV3$_{WT}$ at 42°C.

a, Representative single-channel recordings of TRPV3$_{WT}$-mediated currents at 22°C and 42°C and at +100 mV membrane potential (n = 5; 2,538 were analyzed). **b,** TRPV3$_{WT}$ current-voltage (I-V) relationship at 42°C. The data (mean ± SEM) represent 15 independent experiments and 114,629 events. **c,** Temperature-dependence of P_o recorded at +100 mV (n = 12; 67,673 events were analyzed). Fitting the data allows the temperature coefficient to be estimated, Q_{10} = 26.9 ± 7.4 (n = 19). **d–e**, Structure of TRPV3$_{WT}$-Closed-42°C viewed parallel to membrane (**d**) or intracellularly (**e**) with each of the four subunits colored differently and semi-transparent, the density for the C-terminal domain colored red, and the lipid-like densities colored blue. **f–g**, TRPV3$_{WT}$ pore-forming domains in the closed

(TRPV3$_{WT}$-Closed-42°C, **f**) and sensitized (TRPV3$_{WT}$-Sensitized-42°C, **g**) states with the residues lining the pore shown as sticks. Only two of four subunits are shown; the front and back subunits are omitted for clarity. The pore profiles are shown as space-filling models (grey). Residues in the closed state TRP helix form the C-terminal part of S6 in the sensitized state (red arrows).

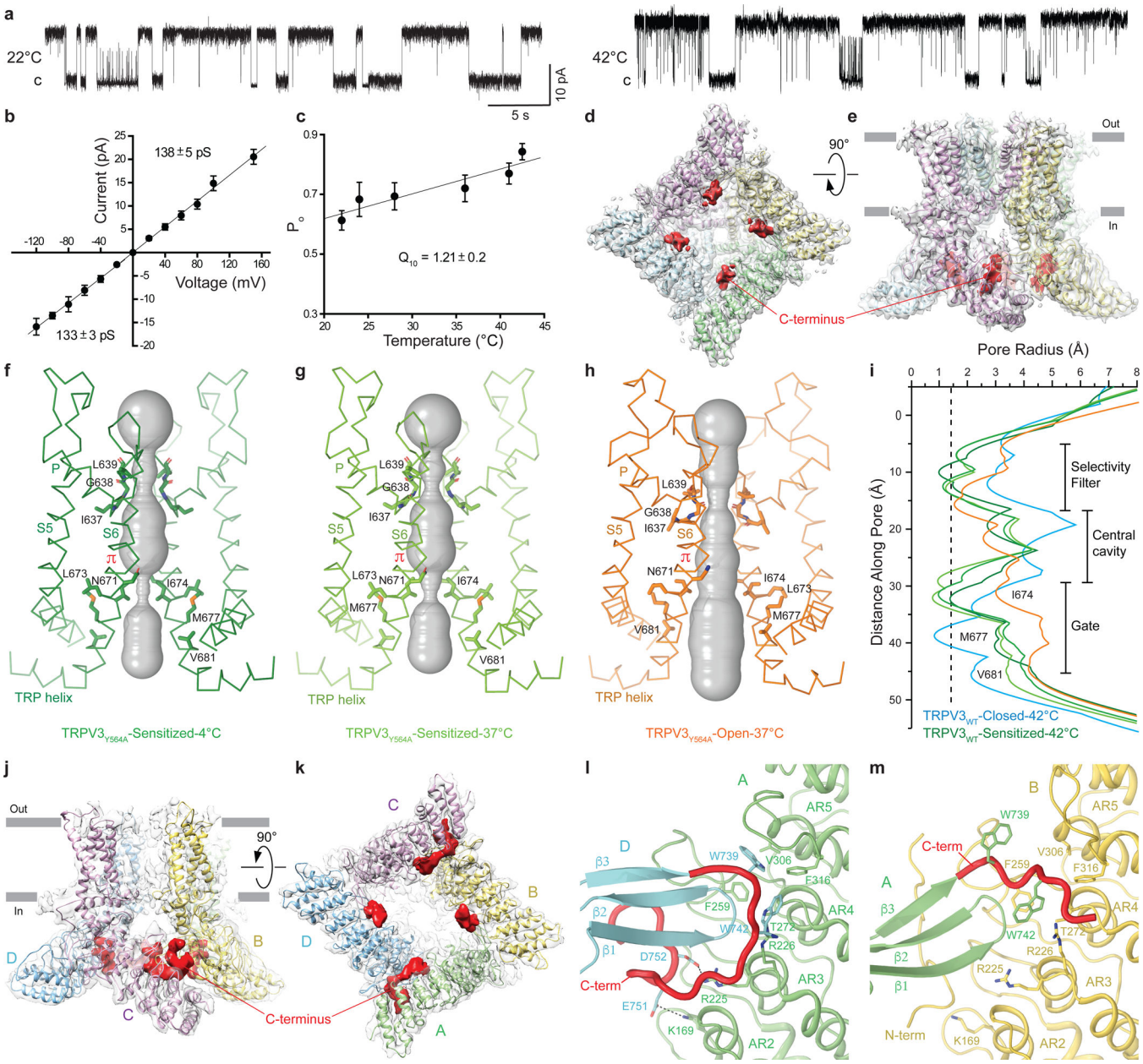

Figure 2. Functional characterization and structures of TRPV3$_{Y564A}$ at 4°C and 37°C.

a, Representative single-channel recordings of TRPV3$_{Y564A}$-mediated currents at 22°C and 42°C and at +100 mV membrane potential (n = 5; 2,538 events were analyzed). **b,** TRPV3$_{Y564A}$ current-voltage (I-V) relationship at 22°C. The data (mean ± SEM) represent 15 independent experiments and 114,629 events. **c,** Temperature-dependence of P_o recorded at +100 mV (n = 12; 67,673 events were analyzed). Fitting the data yields the temperature coefficient, Q_{10} = 1.21 ± 0.20 (n = 21). **d–e**, Structure of TRPV3$_{Y564A}$-Open-37°C viewed parallel to membrane (**d**) or intracellularly (**e**) with each of the four subunits colored differently and semi-transparent, and the density for the C-terminal domain colored red. **f–h**, Pore-forming domain of TRPV3$_{Y564A}$ in the sensitized (TRPV3$_{Y564A}$-Sensitized-4°C, **f**; TRPV3$_{Y564A}$-Sensitized-37°C, **e**) and open (TRPV3$_{Y564A}$-Open-37°C, **h**) states with

residues lining the pore shown as sticks. Only two of four subunits are shown; the front and back subunits are omitted for clarity. The pore profiles are shown as space-filling models (grey). **i**, Pore radii calculated using HOLE[29] for $TRPV3_{WT}$-Closed-42°C (blue), $TRPV3_{WT}$-Sensitized-42°C (dark green), $TRPV3_{Y564A}$-Sensitized-4°C (green), $TRPV3_{Y564A}$-Sensitized-37°C (light green) and $TRPV3_{Y564A}$-Open-37°C (orange). The vertical dashed line denotes the radius of a water molecule, 1.4 Å. **j–k**, $TRPV3_{Y564A}$-Intermediate-37°C viewed parallel to membrane (**j**) or intracellularly (**k**). **l–m**, Expanded views of the intersubunit interfaces between subunits D and A (**l**) and A and B (**m**). The C-terminus is highlighted in red and thickened for clarity. Conserved residues at the C-terminus-ARD interfaces are shown as sticks.

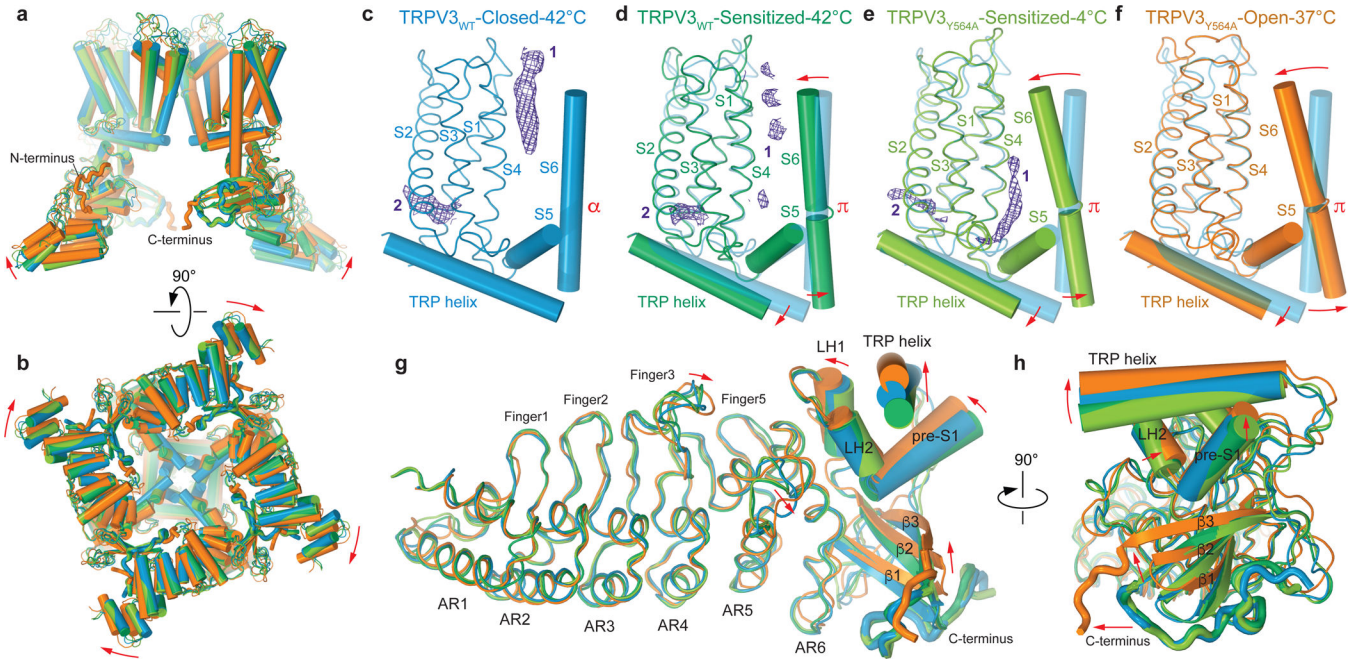

Figure 3. Conformational changes in response to heat.

a–b, Overall superposition of $TRPV3_{WT}$-Closed-42°C (blue), $TRPV3_{WT}$-Sensitized-42°C (dark green), $TRPV3_{Y564A}$-Sensitized-4°C (light green) and $TRPV3_{Y564A}$-Open-37°C (orange) structures viewed parallel to membrane (**a**) or intracellularly (**b**). Only two of four subunits are shown in **a**; the front and back subunits are omitted for clarity. **c–f**, The S1–S5 and TRP helix of one subunit and S6 of the adjacent subunit from $TRPV3_{WT}$-Closed-42°C (**c**) and the same region superposed on $TRPV3_{WT}$-Sensitized-42°C (**d**), $TRPV3_{Y564A}$-Sensitized-4°C (**e**) and $TRPV3_{Y564A}$-Open-37°C (**f**). The densities at sites 1 and 2 are shown as purple mesh. Domain movements relative to the closed state are indicated by red arrows. **g–h**, Superposition of TRPV3 structures based on the ARD. The C-terminus is thickened for clarity. Domain movements relative to the closed state are indicated by red arrows.